PIN OR NEEDLE FRAGMENT HR-3031 - TIN BRONZE - LATE BRONZE AGE - SWITZERLAND

Artefact name	Pin or needle fragment HR-3031
Authors	Marianne. Senn (EMPA, Dübendorf, Zurich, Switzerland) & Christian. Degrigny (HE-Arc CR, Neuchâtel, Neuchâtel, Switzerland) & Naima. Gutknecht (HE-Arc CR, Neuchâtel, Neuchâtel, Switzerland) & Rémy. Léopold (HE-Arc CR, Neuchâtel, Neuchâtel, Switzerland)
Url	/artefacts/1232/

The object

Credit Laténium.

Fig. 1: Pin or needle fragment (after Rychner-Faraggi 1993, plate 74.11),

Credit HE-Arc CR, L.Rémy.

Fig. 2: Dark grey and dark green corrosion products (detail) of the pin or needle fragment near the top,

Credit HE-Arc CR, L.Rémy.

Fig. 3: Dark green corrosion product and sediments (detail) of the pin near the tip,

Description and visual observation

Description of the artefact	Pin or needle fragment (Fig. 1) with dark grey to dark green corrosion products (Figs. 2 & 3). Dimensions: L = 9cm; Ø = 2.5-2.9mm; WT = 3.6g.
Type of artefact	Jewellery
Origin	Hauterive - Champréveyres, Neuchâtel, Neuchâtel, Switzerland
Recovering date	Excavation 1983-1985, object from layer 1 (containing material from the Bronze Age until the 20th century)
Chronology category	Late Bronze Age
chronology tpq	1050 B.C.
chronology taq	800 B.C.
Chronology comment	Hallstatt A2/B
Burial conditions / environment	Lake
Artefact location	Laténium, Neuchâtel, Neuchâtel
Owner	Laténium, Neuchâtel, Neuchâtel
Inv. number	Hr 3031
Recorded conservation data	Not conserved

Complementary information

Considered to be a land patina by Schweizer (1994). The object was sampled in 1987 for analysis. Documentation of the strata in binocular mode on the remaining fragment of the object was performed in 2022.

Study area(s)

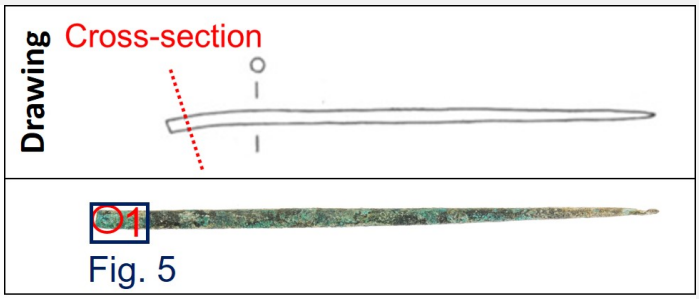

Credit HE-Arc CR, L.Rémy.

Fig. 4: Location of cross-section on drawing and indication of XRF analysis (red circle) and Fig. 5 (blue square),

Credit Laténium, C.Cevey.

Fig. 5: Blue-green corrosion product (detail) of the pin from Fig. 4 with location of Fig. 6 (red square),

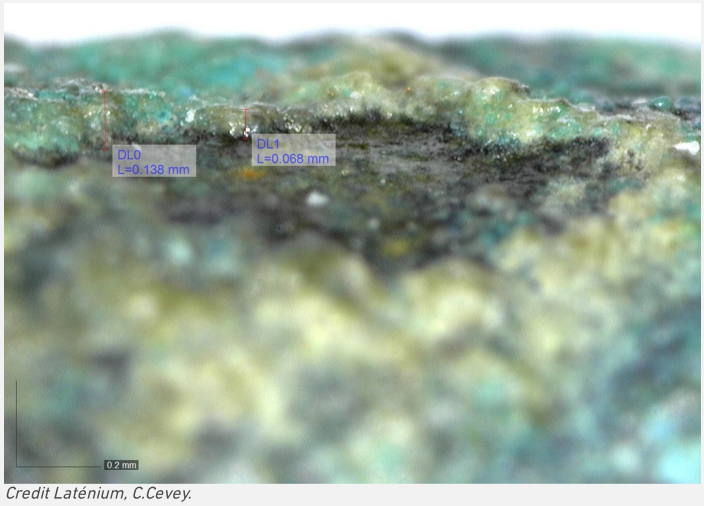

Credit Laténium, C.Cevey.

Fig. 6: Side view of the lacuna of Fig. 5,

Binocular observation and representation of the corrosion structure

The schematic representation below gives an overview of the corrosion structure encountered on the pin from a first visual macroscopic observation.

Strata	Type of stratum	Principal characteristics
S1	Sediments	Nodule, light brown, thin, scattered, non compact, friable, very soft
CP1	Corrosion product	Layer, light brown, thin, discontinuous, compact, powdery, soft
CP2	Corrosion product	Layer, light green, thin, discontinuous, compact, powdery, soft
CP3	Corrosion product	Layer, dark green, thin, discontinuous, compact, tough, soft
CP4	Corrosion product	Layer, blue, thin, discontinuous, compact, tough, soft
CP5	Corrosion product	Layer, black, thin, discontinuous, compact, tough, soft
CP6	Corrosion product	Layer, dark red, thin, scattered, non compact, friable, soft
M1	Metal	Dark yellow, thick, compact, soft

Table 1: Description of the principal characteristics of the strata as observed under binocular and described according to Bertholon's method.

Fig. 7: Stratigraphic representation of the corrosion structure of the pin by macroscopic and binocular observation using the MiCorr application with reference to Fig. 8,

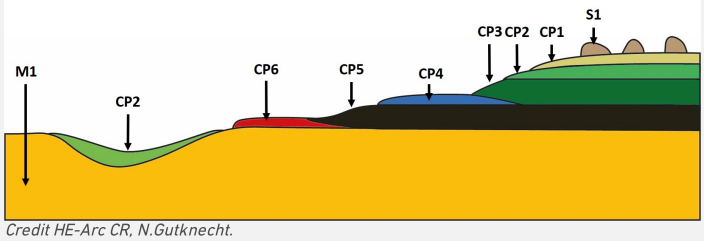

Credit HE-Arc CR, N.Gutknecht.

MiCorr stratigraphy(ies) – Bi

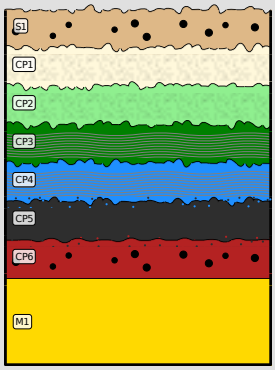

Fig. 8: Stratigraphic representation of the corrosion structure of the pin or needle observed macroscopically under binocular microscope using the MiCorr application with reference to the whole Fig. 7. The characteristics of the strata, such as discontinuity, are accessible by clicking on the drawing that redirects you to the search tool by stratigraphy representation, Credit HE-Arc CR., N.Gutknecht.

Sample(s)

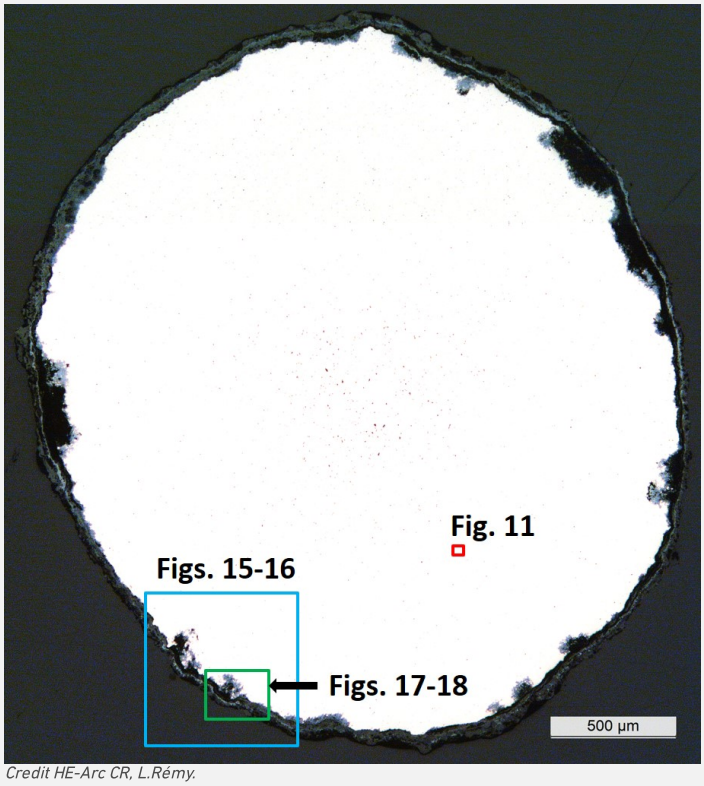

Credit HE-Arc CR, L.Rémy.

Fig. 9: Micrograph of the cross-section of the sample taken from the pin or needle fragment (Fig. 4), unetched, bright field with location of Fig. 11 (red square), Figs. 15 to 16 (blue square) and Figs. 17 to 18 (green square),

Fig. 10: Micrograph of the cross-section of the sample taken from the pin or needle fragment similar to Fig. 9, unetched, dark field,

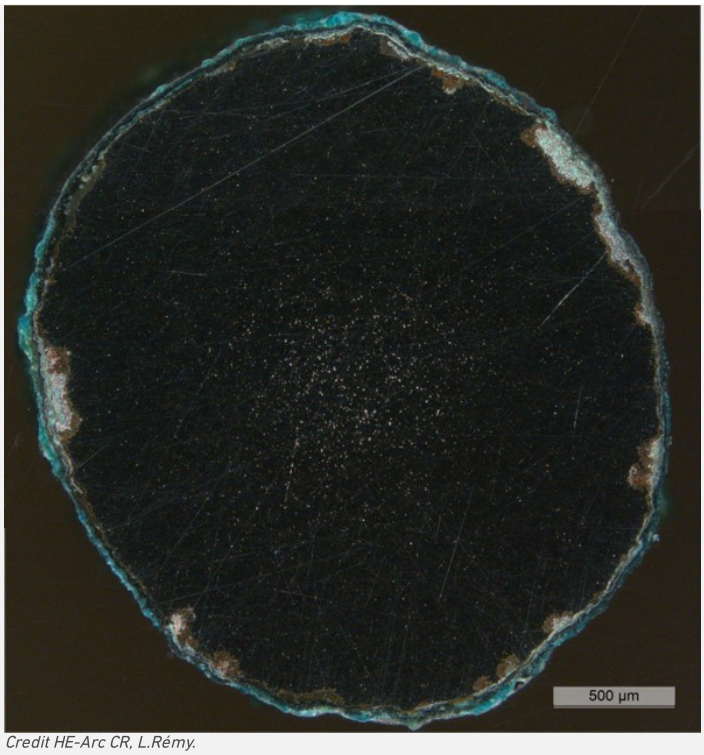

Credit HE-Arc CR, L.Rémy.

Description of sample	The cross-section is circular and is a complete section through the pin (Fig. 9). The surface is completely covered with a rather thin corrosion layer of irregular thickness (Fig. 10). At the center of the cross-section, the metal seems to have more porosities and/or inclusions.
Alloy	Tin Bronze
Technology	Cold worked with partial annealing
Lab number of sample	MAH 87-195
Sample location	Musées d'art et d'histoire, Genève, Geneva
Responsible institution	Musées d'art et d'histoire, Genève, Geneva
Date and aim of sampling	1987, metallography and corrosion characterisation

Complementary information

This sample is mentioned in Schweizer, 1994.

Analyses and results

Analyses performed:

Non-invasive approach

XRF with handheld portable X-ray fluorescence spectrometer (NITON XL5). General Metal mode, acquisition time 60s (filters: Li20/Lo20/M20).

Invasive approach (on the sample)

Metallography (etched with ferric chloride reagent), Vickers hardness testing, ICP-OES (conditions provided in the About tab of the MiCorr application), SEM/EDS (20 keV, Microcity), XRD.

Non invasive analysis

XRF analysis of the pin was carried out on the surface of a representative area next to the cross-section. All strata (soil, corrosion products, and metal) are analyzed at the same time.

The metal is presumably a tin bronze alloy. The other elements detected are: Si, S, Al, Fe, Pb, Sb, As, Ag, Ni, P, Zn.

Elements (mass %)	Cu		Sn		Si		S		Al		Fe		Pb	
	%	+\- 2σ	%	+\- 2σ	%	+\- 2σ	%	+\- 2σ	%	+\- 2σ	%	+\- 2σ	%	+\- 2σ
1	75.5	0.2	9.5	0.05	5.0	0.1	2.0	0.04	2.0	0.2	1.5	0.03	1.0	0.02

Table 2: Chemical composition of the surface of the pin at one representative area shown in Fig. 4. Method of analysis: XRF, UR-Arc CR.

Metal

As suggested by XRF analysis, the remaining metal is a tin bronze with some Sb (Table 3), porosities and small copper sulphide inclusions (Table 4). The etched structure of the tin bronze shows two zones (Fig. 12): more than one half of the section is constituted of re-crystallised and angular grains, some of them with twins (Fig. 13), while the other half shows the presence of strain or slip lines in the grains (Fig. 14). They indicate a final cold working without annealing. Copper sulphide inclusions are found both at the grain boundaries and inside the grains (Figs. 13 and 14). The average hardness of the metal is about HV1 120.

Elements	Cu	Sn	Sb	Ni	As	Pb	Ag	Co	Zn	Fe
mass%	91.29	5.65	1.00	0.69	0.55	0.51	0.22	0.06	0.01	0.02

Table 3: Chemical composition of the metal. Method of analysis: ICP-OES, Laboratory of Analytical Chemistry, Empa.

Elements	S	Cu	Total
mass%	21	85	106

Table 4: Chemical composition of grey inclusions. Method of analysis: SEM/EDS, Laboratory of Analytical Chemistry, Empa.

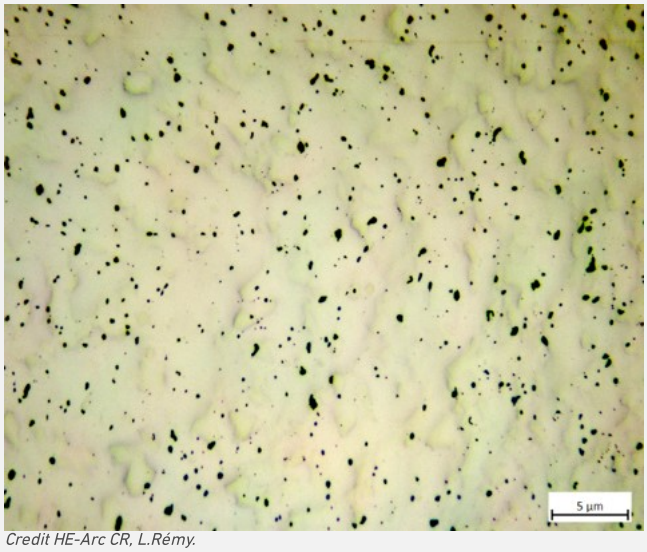

Credit HE-Arc CR, L.Rémy.

Fig. 11: Micrograph of the metal sample from Fig. 9 (detail), unetched, bright field,

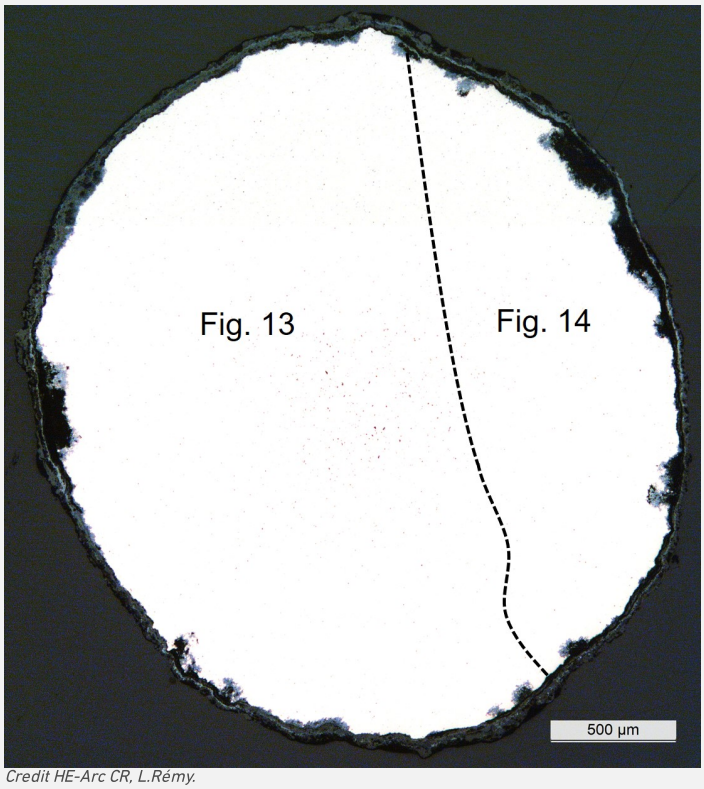

Credit HE-Arc CR, L.Rémy.

Fig. 12: Micrograph similar to Fig. 9 indicating two zones with characteristic microstructures: Fig. 13 where re-crystallised and angular grains with some twins are visible and Fig. 14 where slip lines are more prominent,

Fig. 13: Micrograph of the metal from Fig. 12 (detail), etched, bright field. Twin lines are visible. Grey copper sulphide inclusions are observed, as well as dark porosities,

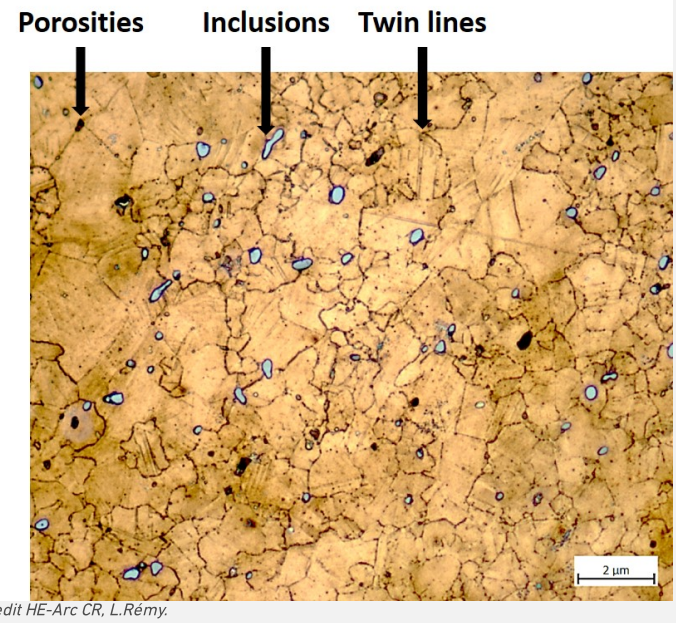

Credit HE-Arc CR, L.Rémy.

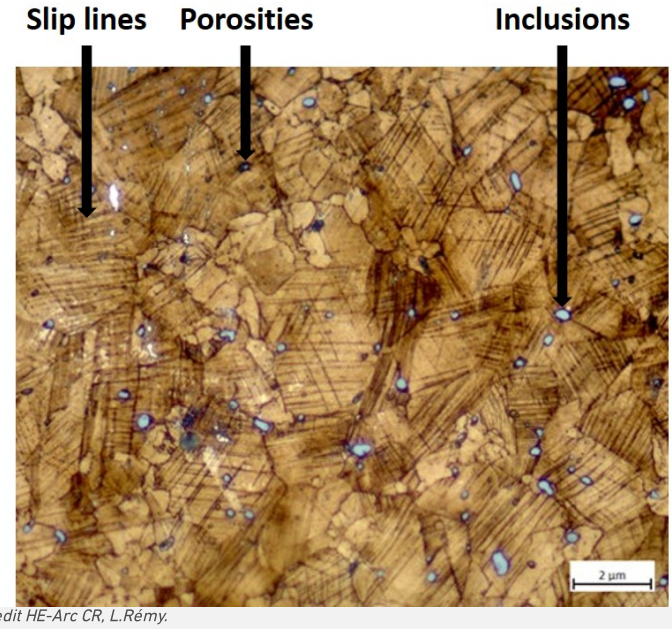

Credit HE-Arc CR, L.Rémy.

Fig. 14: Micrograph of the metal from Fig. 12 (detail), etched, bright field. Polygonal grains with slip lines are observed, as well as grey copper sulphide inclusions and dark porosities,

Microstructure	Polygonal and twinned grains (one half of the cross-section) & slip lines (second half)
First metal element	Cu
Other metal elements	Ni, As, Ag, Sn, Sb, Pb

Complementary information

Schweizer (1994) indicates that the copper-tin alloys similar to the one of the pin have minor constituents that were certainly not added intentionally. Furthermore, he mentions that there is no systematic composition difference between bronzes with a lake patina and those with a land patina.

Corrosion layers

The corrosion layer has an average thickness of about 50µm (Fig. 15). The observation of the sample in cross-section (Figs. 15 and 18) shows the presence of a succession of layers (Figs. 17 and 18): S1 sediment at the top surface, discontinuous layer, black in bright field and light yellow in dark field; CP1 medium continuous layer, extra dark grey in bright field, dark turquoise in dark field; CP2 thin continuous layer, extra light grey in bright field, black in dark field; CP3 thin continuous layer, dark grey in bright field, extra light grey in dark field; CP4 thin continuous layer, extra dark grey in bright field, black in dark field; CP5 thin discontinuous layer, black in bright field, light green in dark field; CP6 medium continuous layer, light grey in bright field, dark orange in dark field; CM1 thin continuous layer;

The EDX elemental mapping (Fig. 20) of SEM image (Fig. 19) of the visually identified strata in cross-section shows the following chemical distribution :
S1 has Al, Ca, Si, and O elements;
CP1 stratum contains Cu, O and S;
CP2 stratum contains Cu, S and Fe;
CP3 stratum contains Sn, O, Fe and S;
CP4 stratum contains Cu, Sn, O, Fe and S;
CP5 stratum contains Cu, Sn, O, Fe and S;
CP6 stratum contains Cu, Sn, O and S.

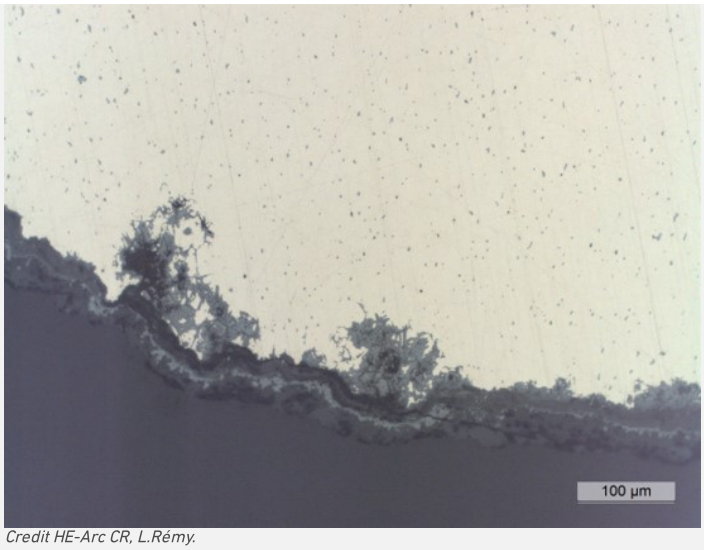

Credit HE-Arc CR, L.Rémy.

Fig. 15: Micrograph of the metal sample from Fig. 9 (detail), unetched, bright field,

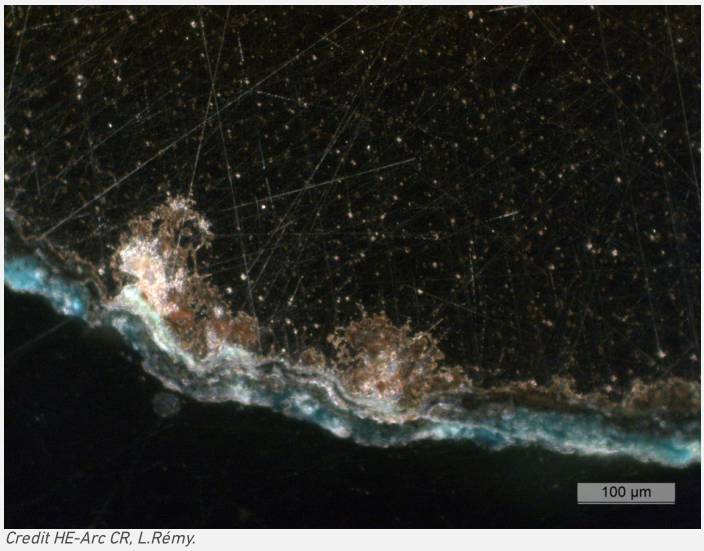

Credit HE-Arc CR, L.Rémy.

Fig. 16: Micrograph of the metal sample similar to Fig. 15, unetched, dark field,

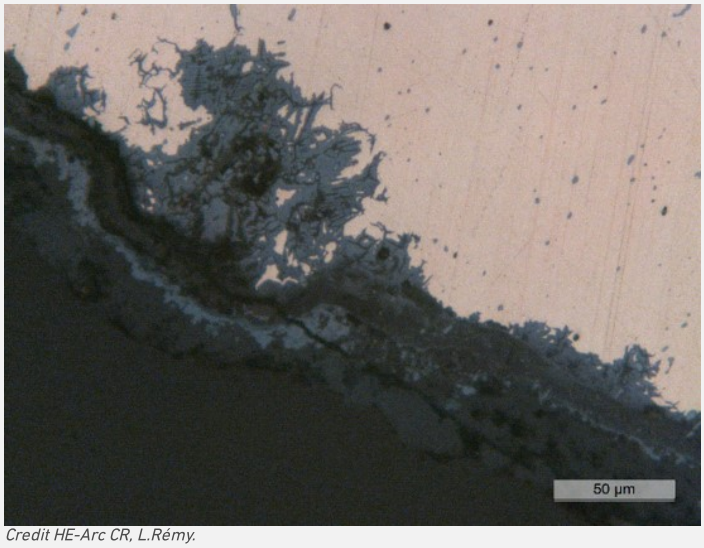

Credit HE-Arc CR, L.Rémy.

Fig. 17: Micrograph of the metal sample from Fig. 9 (detail), unetched, bright field,

Fig. 18: Micrograph of the metal sample similar to Fig.17 (detail), unetched, dark field, and corresponding to the stratigraphy of Fig. 21,

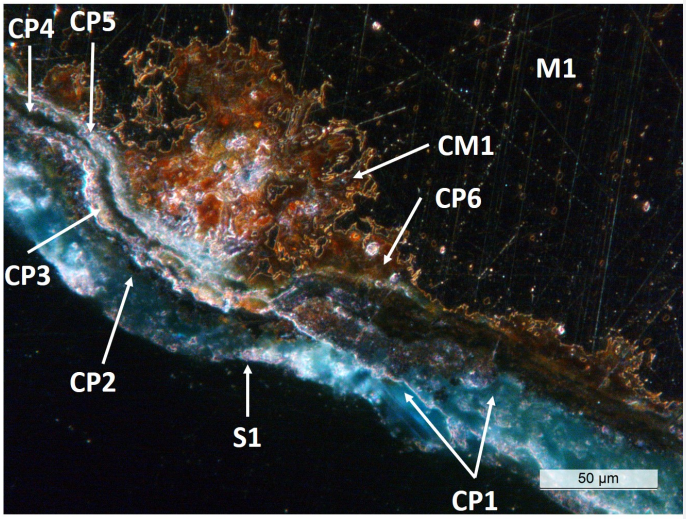

Credit HE-Arc CR, L.Rémy.

Fig. 19: SEM image, BSE-mode from Fig. 17 (detail, reversed and rotated). Method of examination: SEM/EDS, Microcity,

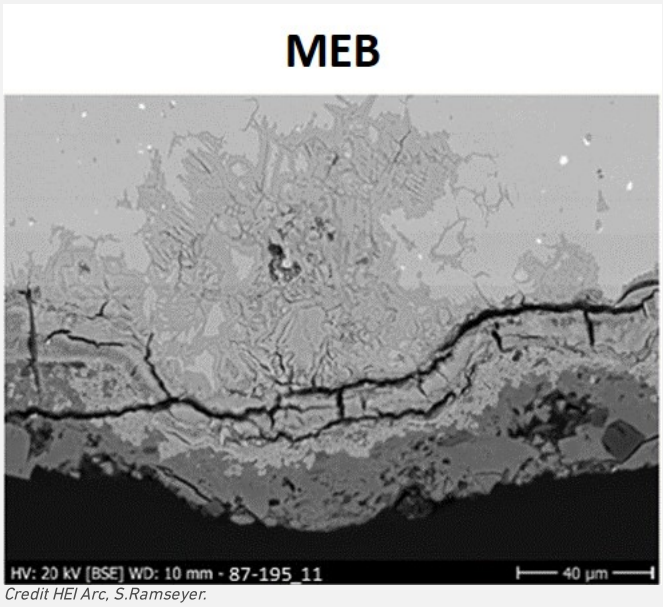

Credit HEI Arc, S.Ramseyer.

Fig 20: Elemental chemical distribution of Fig. 19. Method of examination: SEM/EDS, Microcity,

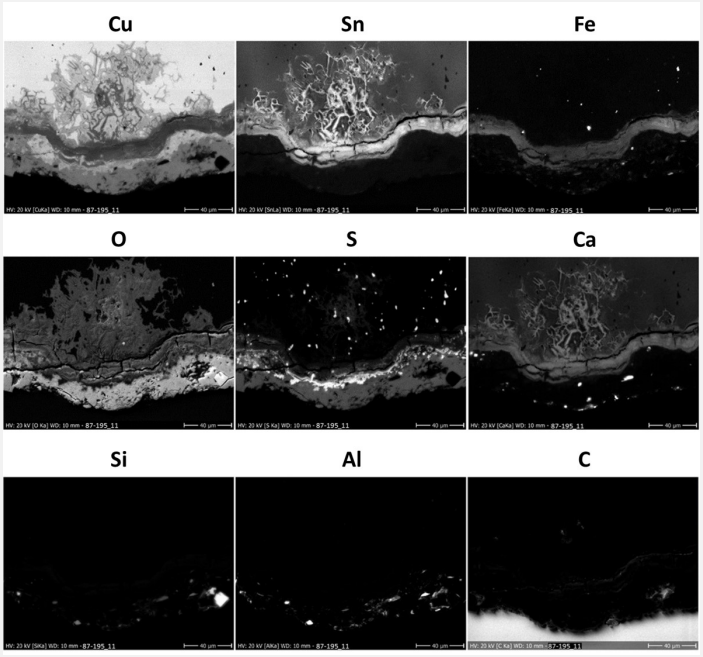

Credit HEI Arc, S.Ramseyer.

Corrosion form	Multiform - pitting
Corrosion type	Type II (Robbiola)

Complementary information

None.

MiCorr stratigraphy(ies) – CS

Fig. 21: Stratigraphic representation of the sample taken from the pin or needle fragment with green-blue patina in cross-section (dark field) using the MiCorr application. The characteristics of the strata are only accessible by clicking on the drawing that redirects you to the search tool by stratigraphy representation. This representation can be compared to Figs. 18 and 20, Credit HE-Arc CR, L.Rémy.

Synthesis of the binocular / cross-section examination of the corrosion structure

Sediment (S1) in binocular mode is documented as sediment (S1) in cross-section mode.
CP1, CP2, CP3 and CP4 in binocular mode are differentiated by their color. They match CP1 in cross-section mode.
CP5 in binocular mode matches CP2, CP3 and CP4 in cross-section mode.
CP6 in binocular mode seems to match CP5, CP6 and CM1 in cross-section mode.
On cross-section, it was possible to describe and analyze the microstructure of the metal.

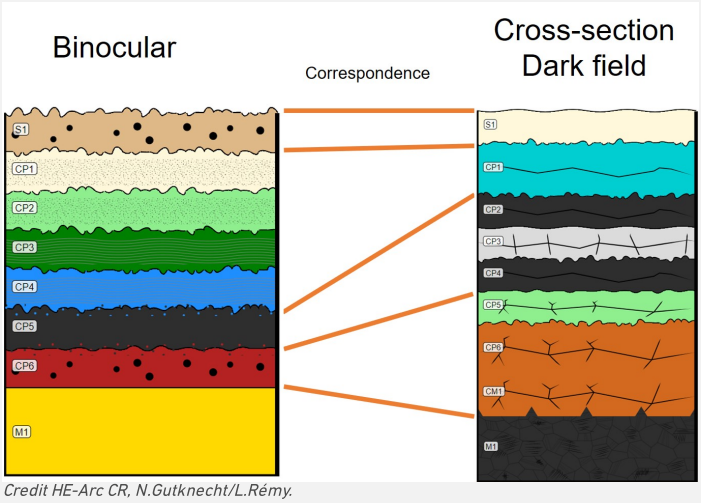

Credit HE-Arc CR, N.Gutknecht/L.Rémy.

Fig. 22: Stratigraphic representation side by side of binocular view and cross-section (dark field),

Conclusion

The pin is made from a tin bronze and has been cold worked and partially annealed. Due to the presence in the corrosion layer of an outer malachite layer (to confirm), the corrosion was described as terrestrial by Schweizer (Schweizer 1994). The elemental chemical distribution of the corrosion layer shows a more complex situation: as expected for an object buried in a terrestrial site, a typical enrichment of Sn is observed in the inner and intermediate layers covering the remaining metal surface. However, it is combined with Fe and O. Cu, S and O are found on top layers. According to Schweizer, these layers were formed in anaerobic conditions and developed later on into malachite in an aerated soil through partial dehydration (Schweizer 1994, Schwartz 1934). The limit of the original surface most probably lies between the Sn-rich inner layer and the Fe/Cu and S-rich outer layers. We refer to type 1 corrosion after Robbiola et al. 1998.

This object was first sampled in 1987. Thanks to an extensive documentation on the cross-section and comparison with similar objects (see references), Schweizer defines a "land patina" typology on this object. In fact it is close to Tang fragment of a knife Hr 6246.

References

References on object and sample

Object files in MiCorr

1. MiCorr_Pin HR-18152
2. MiCorr_Tang fragment of a knife HR-6567
3. MiCorr_Tang fragment of a knife HR-6246
4. MiCorr_Pin HR-17773
5. MiCorr_Pin HR-3071
6. MiCorr_Pin HR-18603
7. MiCorr_Pin HR-3389

References object

8. Rychner-Faraggi A-M. (1993) Hauterive – Champréveyres 9. Métal et parure au Bronze final. Archéologie neuchâteloise, 17 (Neuchâtel), planche 74.11.

References sample

9. Empa Report 137 695/1991, P.O. Boll.
10. Rapport d'examen, Laboratoire Musées d'art et d'Histoire, Geneva GE (1987), 87-194 à 197.
11. Schwartz, G.M. (1934) Paragenesis of oxidised ores of copper, Economic Geology, 29, 55-75.
12. Schweizer, F. (1994) Bronze objects from Lake sites: from patina to bibliography. In: Ancient and historic metals, conservation and scientific resarch (eds. Scott, D.A., Podany, J. and Considine B.B.), The Getty Conservation Institute, 33-50.

References on analytic methods and interpretation

13. Interpretation of orange corrosion products, see: Piccardo P., Mille B., Robbiola L. (2007) Tin and copper oxide in corroded archaeological bronzes, In: Corrosion of metallic heritage artefacts, European Federation of Corrosion Publication n°48, ed. Dillmann et al., 239-262.

14. Robbiola, L., Blengino, J-M., Fiaud, C. (1998) Morphology and mechanisms of formation of natural patinas on archaeological Cu-Sn alloys, Corrosion Science, 40, 12, 2083-2111.